Does Arterial Spin-Labeling MR Imaging–measured Tumor Perfusion Correlate With Renal Cell Cancer Response to Antiangiogenic Therapy in a Mouse Model?

Does Arterial Spin-labeling MR Imaging–measured Tumor Perfusion Correlate with Renal Cell Cancer Response to Antiangiogenic Therapy in a Mouse Model?[1]

Rachel Schor-Bardach, MD
David C. Alsop, PhD
Ivan Pedrosa, MD
Stephanie A. Solazzo, MSc
Xiaoen Wang, PhD
Robert P. Marquis, BS, RT
Michael B. Atkins, MD
Meredith Regan, DSc
Sabina Signoretti, MD
Robert E. Lenkinski, PhD
S. Nahum Goldberg, MD

Purpose: To determine whether arterial spin-labeling (ASL) magnetic resonance (MR) imaging findings at baseline and early during antiangiogenic therapy can predict later resistance to therapy.

Materials and Methods: Protocol was approved by an institutional animal care and use committee. Caki-1, A498, and 786-0 human renal cell carcinoma (RCC) xenografts were implanted in 39 nude mice. Animals received 80 mg sorafenib per kilogram of body weight once daily once tumors measured 12 mm. ASL imaging was performed at baseline and day 14, with additional imaging performed for 786-0 and A498 (3 days to 12 weeks). Mean blood flow values and qualitative differences in spatial distribution of blood flow were analyzed and compared with histopathologic findings for viability and microvascular density. *t* Tests were used to compare differences in mean tumor blood flow. Bonferroni-adjusted *P* values less than .05 denoted significant differences.

Results: Baseline blood flow was 80.1 mL/100 g/min ± 23.3 (standard deviation) for A498, 75.1 mL/100 g/min ± 28.6 for 786-0, and 10.2 mL/100 g/min ± 9.0 for Caki-1. Treated Caki-1 showed no significant change (14.9 mL/100 g/min ± 7.6) in flow, whereas flow decreased in all treated A498 on day 14 (47.9 mL/100 g/min ± 21.1) and in 786-0 on day 3 (20.3 mL/100 g/min ± 8.7) ($P = .003$ and .03, respectively). For A498, lowest values were measured at 28–42 days of receiving sorafenib. Regions of increased flow occurred on days 35–49, 17–32 days before documented tumor growth and before significant increases in mean flow (day 77). Although 786-0 showed new, progressive regions with signal intensity detected as early as day 5 that correlated to viable tumor at histopathologic examination, no significant changes in mean flow were noted when day 3 was compared with all subsequent days ($P > .99$).

Conclusion: ASL imaging provides clinically relevant information regarding tumor viability in RCC lines that respond to sorafenib.

[1] From the Minimally Invasive Tumor Therapy Lab (R.S., S.A.S., S.N.G.), Department of Radiology (S.N.G., D.C.A., I.P., X.W., R.P.M., R.E.L.) and Division of Hematology/Oncology (M.B.A.), Beth Israel Deaconess Medical Center, Harvard Medical School, 1 Deaconess Rd, WCC 308-B, Boston, MA 02215; Departments of Statistics (M.R.) and Pathology (S.S.), Brigham and Women's Hospital, Boston, Mass; and Dana-Farber Cancer Institute, Dana-Farber/Harvard Cancer Center Renal Cancer SPORE, Boston, Mass (R.S., D.C.A., I.P., S.A.S., X.W., R.P.M., M.B.A., M.R., S.S., R.E.L., S.N.G.). Received June 16, 2008; revision requested July 18; revision received September 26; accepted December 8; final version accepted February 16, 2009. R.S. supported by a fellowship grant from the American Physicians Fellowship for Medicine in Israel. **Address correspondence to** S.N.G. (e-mail: *sgoldber@bidmc.harvard.edu*).

The treatment of vascular tumors, and in particular renal cell carcinoma (RCC), has undergone a radical change due to the advent of targeted therapies such as sorafenib that block signaling through the vascular endothelial growth factor (VEGF) receptor (1). Sorafenib, a multikinase inhibitor with potent antiangiogenic effects, has shown substantial clinical activity in patients with advanced RCC and has recently been approved by the U.S. Food and Drug Administration for this indication (2). Sorafenib produces tumor shrinkage in up to 80% of patients with advanced RCC and significantly extends median progression-free survival (2). Other tyrosine kinase inhibitors, such as sunitinib, or the anti-VEGF antibody bevacizumab also have similar antitumor effects (3–6).

Despite these impressive results, sorafenib does not produce complete or durable responses, and most tumors become refractory to treatment within 5–10 months of initiating therapy (7). The mechanism of this resistance is poorly understood but likely includes a component of non-VEGF–mediated angiogenic escape (8). Thus, although this drug is beneficial, resistance to antiangiogenic agents appears inevitable. Yet the nature of this resistance is conjectural, and the ability to detect it before clinically important disease progression is documented remains limited, to our knowledge. The variable response to sorafenib compounds this problem. For example, we observed in unpublished results from our laboratory that three histologically different human clear cell RCC xenografts had very different responses to sorafenib (Caki-1 was resistant; A498 was sensitive for ≥ 4 weeks; and 786-0 showed early response followed by rapid development of resistance by day 5.) This observation highlights the need to develop surrogate markers of treatment effect that adequately assess the effects of treatment on tumor physiology.

Traditionally, therapeutic response has been assessed by using serial tumor size measurements, most notably by using Response Evaluation Criteria in Solid Tumors guidelines (9). However, preclinical assessment of new therapeutics such as antiangiogenic agents has highlighted the limitations associated with standard morphologic measurements. Thus, tumor response may be better assessed by using alterations in vascular supply, rather than size, and functional measurements may therefore be more appropriate (10–12).

One potential imaging strategy to achieve these goals is arterial spin-labeling (ASL) magnetic resonance (MR) imaging, a technique that magnetically inverts or saturates the magnetization of inflowing arterial blood and uses this change as an endogenous tracer. This approach, therefore, excludes the need for an intravenous bolus contrast material injection and enables repeat testing (13). Along these lines, De Bazelaire et al (14) showed the ability of ASL to document changes in RCC metastases receiving the VEGF receptor inhibitor PTK787. They were further able to correlate the early changes in ASL signal intensity 1 month following therapy with tumor size changes at 4 months. The purpose of our study was therefore to determine whether ASL MR imaging can depict and help characterize early changes in the therapeutic response to antiangiogenic therapy (ie, reduction in blood flow or changes in tumor growth pattern) and whether ASL findings early in the course of therapy can be used to predict later therapeutic responses in a mouse tumor model.

Advances in Knowledge

- Arterial spin-labeling (ASL) MR imaging provides spatial and temporal information regarding tumor viability and vascularity, as manifested by tight radiologic-pathologic comparison to intratumoral necrosis and microvascular density immunostaining.
- ASL MR perfusion imaging enables detection of changes in tumor blood flow up to 3 weeks earlier than is possible with currently available clinical criteria (eg, Response Evaluation Criteria in Solid Tumors guidelines) in the A498 renal cell carcinoma (RCC) tumor model.
- Low baseline perfusion (ie, <15 mL/100 g/min) at ASL MR imaging may predict a lack of responsiveness to antiangiogenic therapy.

Implication for Patient Care

- ASL MR imaging may provide predictive and prognostic information for treating patients with RCC with antiangiogenic therapy.

Materials and Methods

The study protocol was approved by the institutional animal care and use committee of Beth Israel Deaconess Medical Center prior to study initiation. Bayer (West Haven, Conn) supplied us with the drug for this study (sorafenib, BAY 43-9006) free of charge. The authors had control of the data and the information submitted for publication.

Experimental Models

Three human RCC xenografts (15) (Caki-1, A498, and 786-0) were used for the study and were implanted in mouse models that were previously shown to optimally grow these lines. Caki-1 (n = 6)

Published online
10.1148/radiol.2521081059

Radiology 2009; 251:731–742

Abbreviations:
ASL = arterial spin labeling
RCC = renal cell carcinoma
VEGF = vascular endothelial growth factor

Author contributions:
Guarantors of integrity of entire study, R.S., S.N.G.; study concepts/study design or data acquisition or data analysis/interpretation, all authors; manuscript drafting or manuscript revision for important intellectual content, all authors; manuscript final version approval, all authors; literature research, R.S., R.E.L., S.N.G.; experimental studies, R.S., D.C.A., I.P., S.A.S., X.W., R.P.M., S.S., R.E.L., S.N.G.; statistical analysis, R.S., M.R., R.E.L., S.N.G.; and manuscript editing, R.S., D.C.A., I.P., M.B.A., S.S., R.E.L., S.N.G.

Funding:
This research was supported by National Cancer Institute Dana-Farber/Harvard Cancer Center Renal Center SPORE grants (1 P50 CA10194-01 and 5 R21 CA121570).

See Materials and Methods for pertinent disclosures.

and A498 (n = 11) were implanted in Nu/Nu mice (mean weight, 30 g; age range, 6–8 weeks; Taconic Farms, Germantown, NY). The xenograft 786-0 (n = 22) was implanted in NIH III beige mice (mean weight, 30 g; age range, 6–8 weeks; Taconic Farms). For each cell line, the experimental group received 80 mg of the antiangiogenic agent sorafenib (BAY 43-9006; Bayer) per kilogram of body weight by means of gavage, once daily, 6 days a week, for the duration of the study starting from when the tumors reached 12 mm in diameter (R.S., S.A.S.). This tumor size was chosen to allow follow-up of growth changes and ASL imaging findings over time before the tumors reached a final size of 20 mm (ie, the maximum permitted by the institutional animal care and use committee). ASL imaging was performed at baseline and at scheduled intervals, as noted in Figure 1. Animals were sacrificed for radiologic-pathologic correlation according to the schedule in Figure 1. In the sorafenib groups, tumors were measured daily with calipers following administration of therapy (R.S., S.A.S.). Ten animals served as controls, receiving no sorafenib, during the period of imaging (786-0, n = 4; A498, n = 3; Caki-1, n = 3) and were measured twice a week with calipers.

Sorafenib Administration

Sorafenib (80 mg/kg) was administered daily by oral gavage (R.S., S.A.S.). Sorafenib was dissolved in a 50% cremophor EL (Sigma, St Louis, Mo)–50% ethanol (Pharmaco Products, Brookfield, Conn) mixture. The compounds were sonicated for 5–10 minutes. Once in solution, the aqueous component (75% water) was gradually added and diluted to generate the final dosing solution (1). Each dose of sorafenib was weighed and stored in dry form away from light and was dissolved to liquid form immediately prior to administration.

Tumor Induction

Tumor cells were initially maintained in the appropriate culture media (Dulbecco's modified Eagle's medium [Mediatech, Herndon, Va] for 786-0, McCoy's 5A [Mediatech] for Caki-1, and Eagle minimum essential medium [ATCC, Manassas, Va] for A498) and were grown on plates until confluent. Three to five million cells were obtained per injection. Cultures were dissolved by using cell dissociation solution (Sigma-Aldrich, St Louis, Mo), and tumor cells were then suspended in sterile phosphate-buffered saline (Mediatech) for a total volume of 0.4 mL per injection. A 20-gauge needle was used for subcutaneous left flank injection of each animal. Following tumor inoculation, animals were monitored every 3–4 days to measure tumor growth. Treatment was initiated when the tumors reached a desired size of 12 mm. Cell culture, tumor induction, monitoring, and randomization were performed by two authors (R.S., S.A.S.). On completion of the study, the animals were euthanized by means of barbiturate overdose (Nembutal Sodium Solution; Abbott Laboratories, North Chicago, Ill) according to institutional animal care and use committee guidelines.

ASL MR Imaging

ASL perfusion MR imaging was performed on days 0 and 14 in treated and control animals for all three lines: Caki-1 (n = 6), A498 (n = 6), and 786-0 (n = 7). To enable imaging at times of growth, on the basis of the different growth patterns of each cell line, additional imaging time points were chosen. Imaging on days 3, 5, 6, 9, and 22 was performed for 786-0 tumors (n = 15), and multiple weekly follow-up studies were performed in five A498-bearing mice receiving therapy for 4–12 weeks (ie, until tumors had grown at least 3 mm larger than at baseline), for a total of an additional 45 studies for the A498 model. Thus, a total of 79 ASL MR imaging studies were performed and processed.

Mice were imaged with a 3.0-T whole-body clinical imager (3T HD; GE Healthcare Technologies, Waukesha, Wis) with a receive-only custom-built surface coil of approximately 3 cm in diameter placed below the animal. Transmission was performed with the product body coil. After anesthesia was induced with an intraperitoneal injection of 1:10 diluted pentobarbital (Nembutal Sodium Solution; Abbott Laboratories), at a dose of 5 mg/kg, mice were placed in the prone position on the magnet table and were restrained to limit movement. When necessary to maintain adequate anesthesia, booster anesthetic injections at one-tenth of those doses were administered intraperitoneally (R.S.).

ASL Technique

Initially, a three-axis scout study was performed to identify the tumor for planning purposes by using an echo time of 1.7 msec, a repetition time of 7.8 msec, a 30° flip angle, and a 31.2-kHz

Figure 1

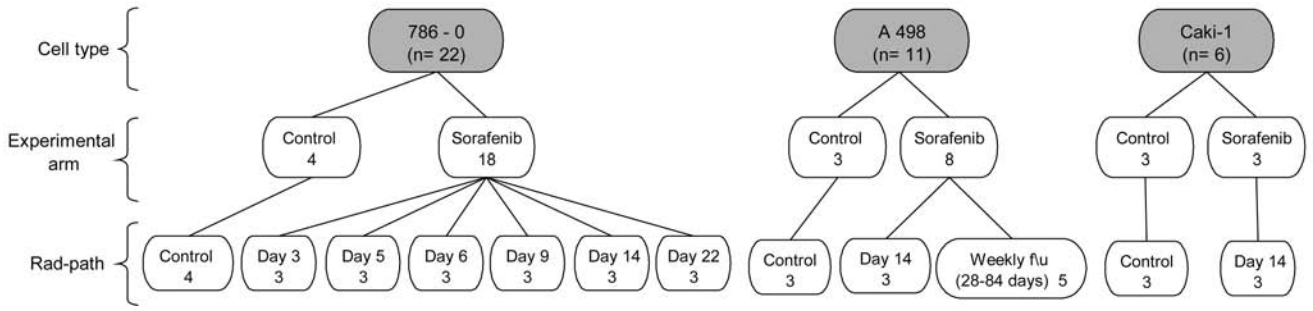

Figure 1: Experimental groups and design. *Rad-path* denotes that both ASL MR imaging and histopathologic examination were performed, as described in the text. For the A498 follow-up *(f/u)* group, all five animals were imaged weekly for various periods until growth of 3 mm was noted.

bandwidth. A 38-cm field of view with a 256 × 128 matrix, a section thickness of 4 mm with 7.5-mm spacing, and five sections per direction were selected. Two signals were acquired.

ASL perfusion was performed by using a background-suppressed flow-sensitive alternating inversion-recovery strategy (16,17). A 3-cm slab centered on the section was presaturated with repeated 90° pulses just before the labeling inversion pulse, a frequency-offset-corrected inversion pulse (18,19), was applied 2500 msec before imaging. This inversion pulse was alternated between selective and nonselective for successive image acquisitions by turning off or on the associated gradient pulse. Additional, nonselective adiabatic inversion pulses at 2001, 1089, 445, and 105 msec were applied to achieve background suppression (20). Inferior and superior saturation pulses were applied centered at 1000, 713, and 217 msec to suppress unlabeled signal at the imaging time and to make quantification insensitive to arrival time (21,22).

Images were acquired in a single, 2-mm axial section at the greatest tumor diameter. Single-shot fast spin-echo images (ie, imaging performed every excitation) were acquired with a 128 × 128 matrix on an 8-cm field of view. A repetition time of 5 seconds between images (ie, the repeated alternation between selective and nonselective inversion to increase the signal-to-noise ratio) and a bandwidth of 20.8 kHz were selected. Twenty-four label and control pairs were acquired and averaged for the ASL acquisition.

To provide anatomic landmarks, ASL sequences were followed by T1 measurements by using the same imaging sequence but with inversion recovery at different inversion times.

The T1 measurement was performed with inversion times of 50, 100, 200, 300, 400, 500, 600, 800, 1000, 1200, and 1400 msec. The time between single-shot images was determined by using manual switching of inversion time but was always longer than 15 seconds. A reference proton density image was acquired by turning off all background suppression and labeling pulses in the ASL preparation. For each animal, the ASL acquisition was 4 minutes, and the acquisition of additional reference and T1 images required an additional 2 minutes.

Image Processing

ASL produces a signal intensity change, which reflects the competition between inflowing labeled water in blood and the decay of that signal with T1. Knowledge of the timing of the labeling, the T1, and the sensitivity of the MR imager to water, as measured on a proton density image, permit quantification of blood flow with relatively simple equations (14,22).

All imaging signals were saved as raw echo amplitudes and were transferred to a workstation for reconstruction. This reconstruction permitted complex averaging of label and control images. The ASL difference image, between average label and control images, was then converted to quantitative blood flow (BF) by using the following equation (14,22):

$$\mathrm{BF} = \frac{\lambda(S_{\mathrm{sel}} - S_{\mathrm{nonsel}})}{2\alpha(\mathrm{TI} - T_{\mathrm{sat}})S_{\mathrm{ref}}} e^{\mathrm{TI}/\mathrm{T1}}.$$

Here, S is the signal for the nonselective (S_{nonsel}) and selective (S_{sel}) ASL images and the reference proton density image (S_{ref}). TI is the inversion time, 2500 msec; T_{sat} is the time of the first saturation pulse, 1000 msec before imaging; T1 is the T1 of blood, assumed to be 1500 msec; α is the inversion efficiency, assumed to be 1.0; and λ is the tissue-blood partition coefficient, assumed to be 1 mL/g. In humans, α has been measured at approximately 0.75 because of the repeated background-suppression pulses (20), and λ in brain tissue averages 0.9. If we had used these human values for these unmeasured quantities, calculated blood flow would have been 20% higher. The use of the T1 of blood, and not the T1 of tissue, in the calculation assumes that the label spends most of the 2500 msec after inversion in the arteries and microvasculature. Because this assumption is probably true, and because the T1 of the tumor was typically only slightly shorter, the use of blood T1 probably did not affect the accuracy of quantification. The blood

Figure 2

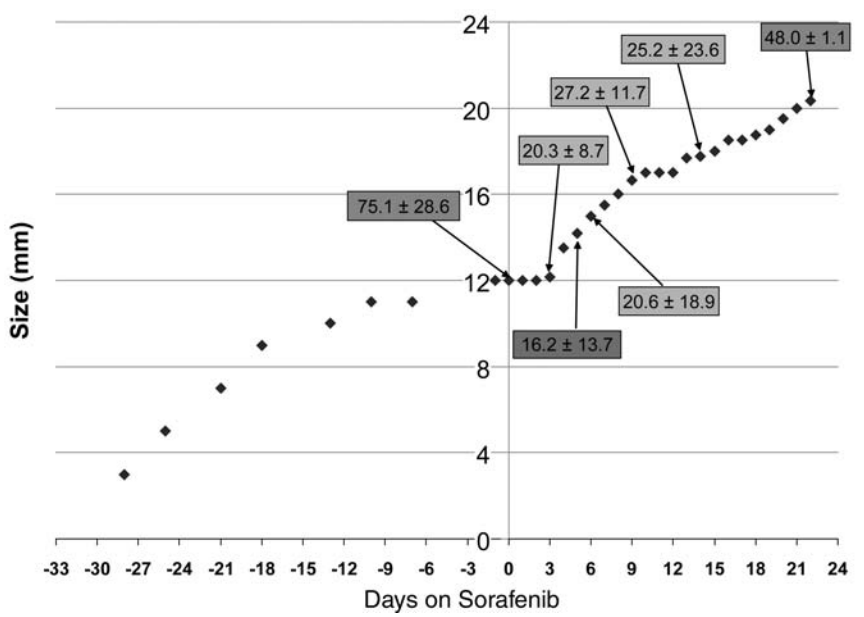

Figure 2: Average growth curve of 786-0 cell line. Size was measured daily with calipers; mean blood flow values (in mL/100 g/min) in shaded boxes were calculated from ASL MR images. Unlike changes in spatial blood flow distribution (see Fig 3), no significant change was seen in mean blood flow from day 3 to 22, despite measured tumor growth.

Figure 3

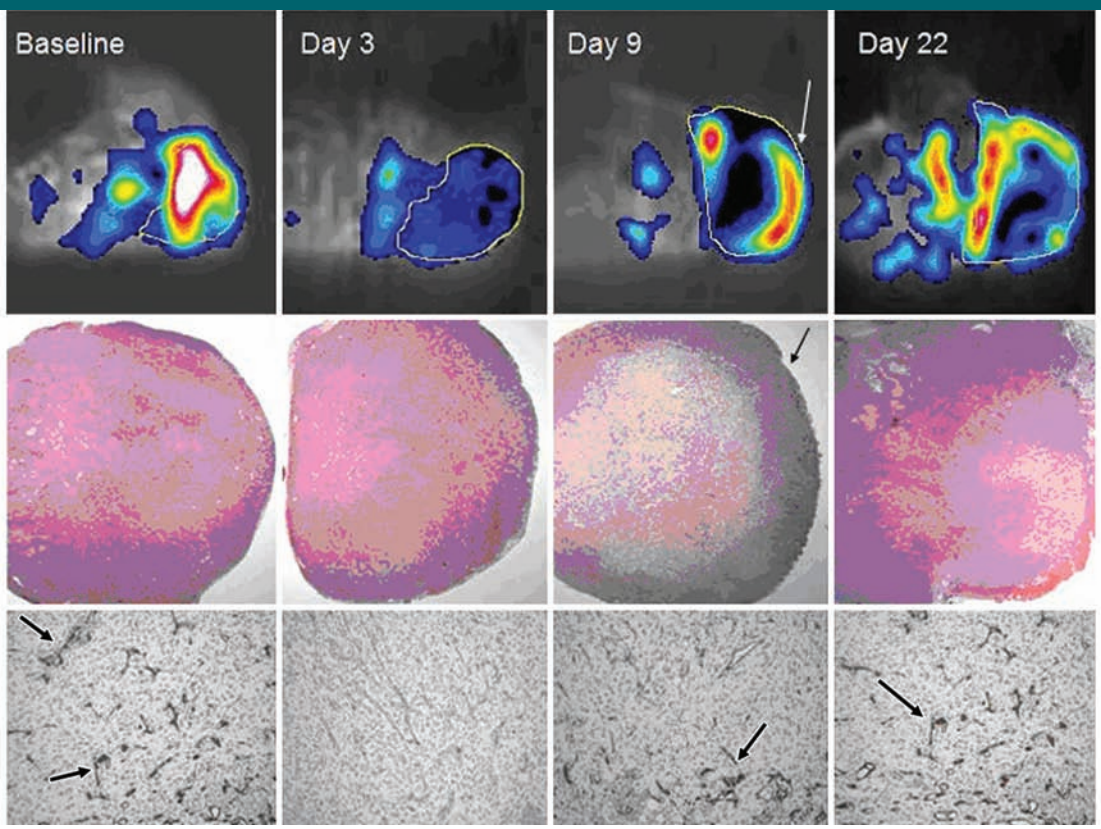

Figure 3: Histopathologic correlation of sorafenib-treated 786-0 tumors with ASL perfusion maps. Top row: ASL perfusion maps (with yellow region of interest outlining the tumor). Middle row: Hematoxylin-eosin–stained specimens (entire specimen is tumor) (original magnification, ×2). Bottom row: Immunohistochemistry images. (CD34 stain; original magnification, ×20.) ASL map shows decreased signal intensity on day 3 with return of peripheral signal intensity (arrow in top row) from day 9 to day 22. Viability (dark pink on day 9 that surrounds lighter necrosis, arrow in middle row) and vessels (brown-stained structures on immunohistochemistry images, arrows in bottom row) correlated with new ASL signal intensity on days 9 and 22.

flow was calculated according to the above equation on a pixel-by-pixel basis, and quantitative maps were produced (14,22).

The quantitative maps and the corresponding proton density reference images were then analyzed by using software (ImageJ, Image Processing and Analysis in Java; National Institutes of Health, Bethesda, Md, *http://rsb.info.nih.gov/ij/*) (R.S. and D.C.A., with 1 year of clinical experience and more than 18 years of research experience, respectively, in body MR image interpretation). To determine tumor perfusion, a region of interest was drawn freehand around the peripheral margin of the tumor by using an electronic cursor on the reference image and was then copied to the perfusion image. The mean blood flow for the tumor tissue within the region of interest was derived, and image window and level were fixed. A 16-color table was applied in 10 mL/100 g/min increments ranging from 0 to 160 mL/100 g/min, with flow values represented as varying shades of black, blue, green, yellow, red, and purple, in order of increasing perfusion. To improve signal-to-noise ratio, the images were smoothed prior to display by using the ImageJ smoothing function, as generally the signal-to-noise ratio of an MR image improves as the full width at half maximum (in pixels) of the smoothing kernel for two-dimensional smoothing.

Histopathologic Correlation

Immediately after the last MR imaging study, the skin was marked where the axial plane had been obtained before the animal was moved from the table. All animals were then euthanized with barbiturate overdose as described previously (within 1 hour). Tumors were sliced immediately in the axial plane, corresponding to the MR-imaging section orientation (and within 10% measurement or 1 mm of the MR imaging diameter), and were stained with hematoxylin-eosin (Fig 1). All tissue specimens were examined by a pathologist (S.S., with 22.7 years of experience) at their greatest axial diameter and at the location of the MR image to identify the presence of both viable and necrotic-appearing cells.

For assessment of microvascular density, paraffin-embedded tissue slices from all specimens were immunostained with a rat monoclonal antibody to the endothe-

lial cell marker CD34 (clone MEC 14.7; Abcam, Cambridge, Mass). Slices were deparaffinized, and, after microwave treatment in antigen unmasking solution for 10 minutes, slices were incubated in 3% hydrogen peroxide for 15 minutes to inactivate endogenous peroxidase. Slices were incubated with the anti-CD34 antibody (dilution, 1:100), and detection was performed by using a rabbit antirat secondary antibody (E0468; Dako, Carpinteria, Calif) (dilution, 1:750) followed by using a horseradish peroxidase detection kit (EnVision+ System; Dako).

Data and Statistical Analysis

For each of the 79 studies, ASL values were analyzed qualitatively (ie, by comparing changes in the spatial distribution of blood flow on serial perfusion maps) and quantitatively as a mean ± standard deviation for tumor blood flow calculated for the entire tumor section by using a statistical program (SAS; SAS Institute, Cary, NC) (R.S.; M.R., with 10 years of experience). Radiologic-pathologic correlation was performed for all harvested tumors (Fig 1). Visual comparison of histologic tissue slices, including semiquantitative microvascular density assessment, with the corresponding ASL MR perfusion images was also performed. Tumor blood flow was analyzed by using linear regression (786-0, Caki-1) or mixed-effects linear regression (A498), depending on the experimental design, and contrasts analogous to *t* tests were used to make pairwise comparisons between time points. Bonferroni-adjusted *P* values less than .05 were considered to denote statistically significant differences.

Results

786-0 Cell Line

From consistent daily growth, tumors stopped growing once given sorafenib therapy for 3–5 days (4.1 days ± 0.8 [standard deviation]) and then grew rapidly while still receiving therapy (Fig 2).

Quantitative tumor blood flow analysis.—At baseline, mean blood flow was 75.1 mL/100 g/min ± 28.6 for the four 786-0 tumors. Blood flow values significantly decreased at 3, 5, and 6 days following therapy (20.3 mL/100 g/min ± 8.7 to 20.6 mL/100 g/min ± 18.9, up to 78.4% decrease, $P < .05$), with only trends for changes in mean blood flow observed for days 9–22 (ranging from 25.2 mL/100 g/min ± 23.6 to 48.0 mL/100 g/min ± 1.1, $P = .06–.08$). Additionally, no statistically significant changes in mean blood flow were noted when we compared the blood flow value on day 3 or day 5, the lowest blood flow values, to that on all subsequent days ($P > .99$). Given that the tumors grew from day 5 to 14, mean blood flow measurements did not correlate with growth (Fig 2).

ASL perfusion maps.—For qualitative measurement, high ASL signal intensity was seen at baseline throughout all 786-0 tumors, with a marked reduction of signal intensity on day 3. On days 5–6, there was an absence of central signal intensity with a return of patchy peripheral signal intensity. A distinct rim was clearly defined for all tumors by day 9; this was followed by continuous extension of the rim and progression of ASL signal intensity to days 14–22 (Fig 3).

Histopathologic correlation.—Microscopic and microvascular density analysis of tissue slices revealed close correlation with the regional distribution of signal intensity on the ASL perfusion maps. At hematoxylin-eosin staining, 786-0 tumor was completely viable and typically highly vascular at baseline (Fig 3).

By day 5 or 6, hematoxylin-eosin staining showed extensive central necrosis with absence of central vessels. Regions of necrosis matched areas of absent perfusion for all specimens beyond day 5. The peripheral viable rim was associated with return of vessels on day 9, with greater extent of tumor viability and vascularity on days 14–22.

The histopathologic examination findings were partially discrepant on day 3, in that, despite significantly low signal intensity on the ASL map, the tumors looked viable at hematoxylin-eosin staining. Nevertheless, microvascular density assess-

Figure 4

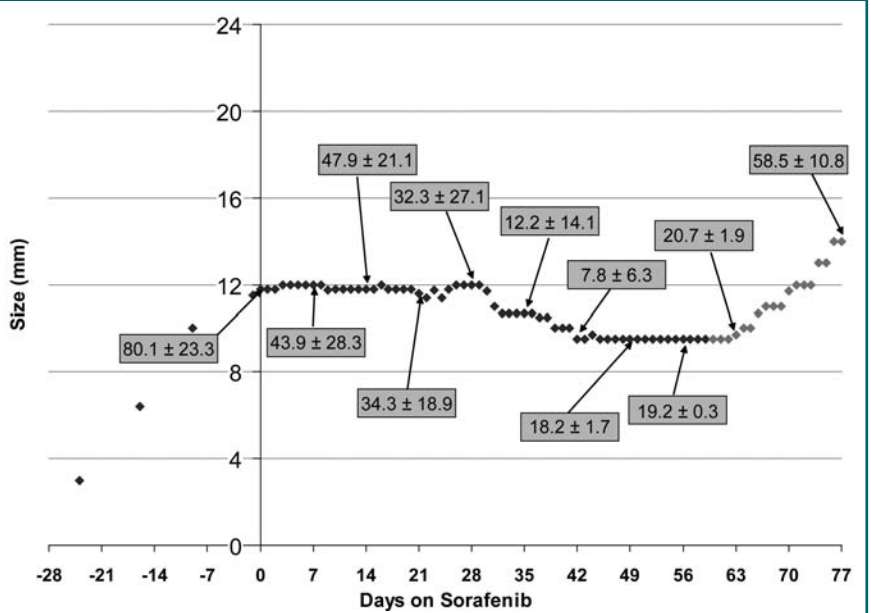

Figure 4: Average growth curve of A498 cell line. Data to day 60 show decreased blood flow and stable or decreased tumor size. Beyond 60 days, growth measurements of a single representative tumor are presented (denoted by lighter gray diamonds), with average blood flow values in animals regrowing to 15 mm. Size was measured daily with calipers; mean blood flow values (in mL/100 g/min) presented in the shaded boxes were calculated from ASL MR images.

Figure 5

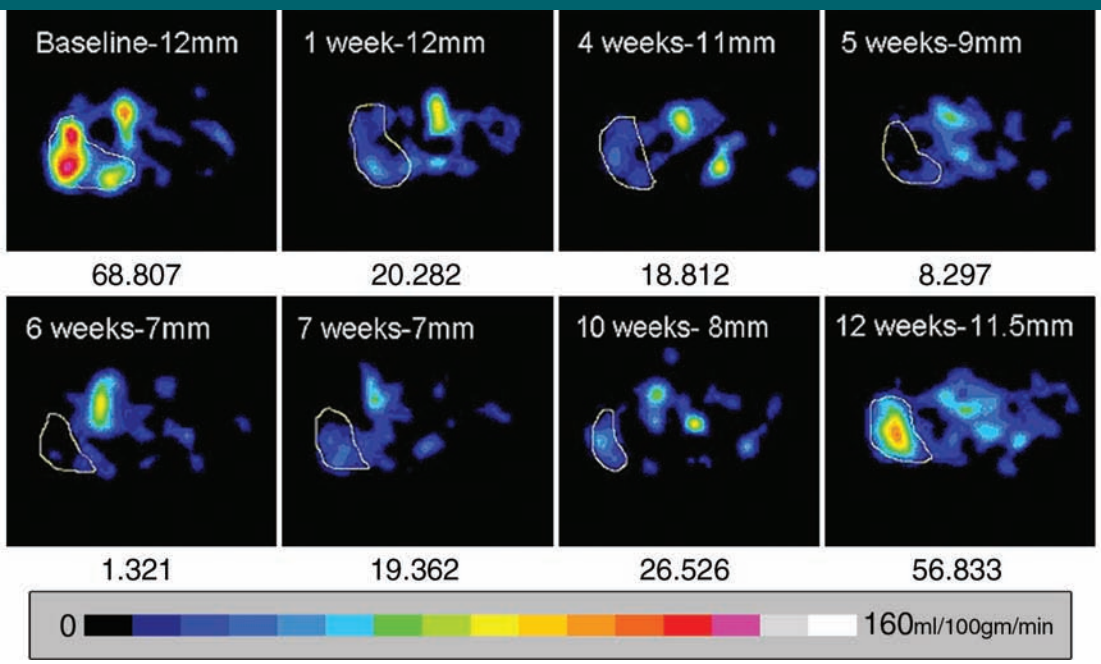

Figure 5: ASL perfusion maps in sorafenib-treated A498 tumors. Yellow region of interest outlines the tumor in each image. Mean blood flow (in mL/100 g/min) is noted below the image. Color table represents flow values. ASL signal intensity is high at baseline, with decrease of both signal intensity and tumor size following therapy. Minimum values are seen at 6 weeks. Yet at 7 weeks, blood flow was up to 19.362 mL/100 g/min, with stable tumor size. Definitive measurable tumor growth was seen at 11 weeks, which was 4 weeks after the reversal of blood flow. *gm* = Gram.

ment revealed only some residual vessels with collapsed or inflammatory-infiltrated lumina with decreased CD34 endothelial cells, which suggests an inability to perfuse this previously vascular tumor.

A498 Cell Line

Tumors were responsive to sorafenib for 4–10 weeks, maintaining size stability (±1 mm for five tumors) or slight regression (of up to 5 mm in three tumors) to a nadir of 4 weeks. Earliest measured growth occurred on days 45–74. For the five animals with long-term follow-up, three tumors were stable and two showed regression of 4 mm (±1 mm) while receiving sorafenib prior to resuming growth.

Quantitative tumor blood flow analysis.—Baseline mean blood flow was 80.1 mL/100 g/min ± 23.3 for A498, with a variable statistically significant decrease in all treated tumors 14 days following therapy (47.9 mL/100 g/min ± 21.1, up to 58.2% decrease, $P = .003$) (Fig 4). With longer follow-up, further decrease in signal intensity was seen, with lowest values measured at 28–42 days of receiving sorafenib (0.44–31.9 mL/100 g/mL), followed by increased blood flow thereafter (58.5 mL/100 g/min ± 10.8 at day 77, after 3 mm of growth; $P < .001$).

ASL perfusion maps.—High baseline ASL signal intensity was seen throughout the entire tumor. On days 14–35, there was central loss of the ASL signal intensity, with almost complete absence at 5–6 weeks following therapy. Patchy gradual return of signal intensity was seen beyond day 42 in the long-term follow-up animals, with this signal intensity return preceding tumor growth by 2–3 weeks (mean, 23 days ± 8; range, 17–32 days) (Fig 5).

Histopathologic findings.—Close correlation was seen between microscopic and microvascular density analysis of tissue slices and data on ASL perfusion maps. A498 tumors were vascular and cystic at baseline, with decreased vascularity and cystic components seen at day 14. CD34 stained many mature vessels at baseline; there was a marked reduction at 14 days following therapy (Fig 6). Regrowing tumors (45–84 days) showed a return of the vessels from the margins toward the center in regions with the greatest return of ASL signal intensity, intermixed with variable amount of necrosis.

Caki-1 Cell Line

This line showed no response to sorafenib, as the growth rate did not change despite therapy (Fig 7). These tumors had low to minimal scattered ASL signal intensity at baseline (10.2 mL/100 g/min ± 9.0), with no significant change seen 14 days following therapy (14.9 mL/100 g/min ± 7.6, $P > .10$). Histopathologic correlation revealed a substantial stromal component, with microvascular density assessment showing minimal vascularity in both the baseline and day-14 specimens (Fig 8).

Discussion

During the past decade, major advances were made in the field of functional imaging techniques. Computed tomographic

(CT) perfusion and MR imaging–based perfusion methods have become more feasible and reproducible. Therefore, the use of imaging for oncologic applications has moved from merely a descriptive tool of size and extent (ie, conventional morphology) to incorporating tumor physiology as an integral component in diagnosis, staging, and characterization of tumor status. Apart from being noninvasive and fast, these perfusion studies provide the opportunity to assess tumor response to antiangiogenic therapy over time, as well as temporal changes in tumor angiogenesis, and offer the ability to noninvasively sample the entire tumor.

Despite the potential of CT perfusion as a noninvasive method for monitoring responses to antiangiogenic therapy, its use for this specific aim has not been completely validated yet, and controversies exist regarding the correlation between CT perfusion parameters and microvascular density, the current histologic marker for assessing angiogenic activity (23,24). A limitation of CT perfusion studies is that separation of blood flow and permeability changes at CT requires more complex models (25) that are not always used and may enhance noise. An additional disadvantage of CT perfusion is that iodinated contrast media may be contraindicated in some cases where preservation of renal function is warranted (26–28), especially if several follow-up studies are needed. Repetitive studies could also potentially raise the problem of accumulated ionizing radiation exposure with CT perfusion.

ASL is a noninvasive imaging modality that electromagnetically labels the spins of water protons in the feeding arteries before they flow into the tissue (13). This method has been validated with reference-standard measures, including microspheres (29) and iodoantipyrine (30). The advantages of ASL include its noninvasive nature, its potential to yield absolute quantification, its ability to interrogate separate vascular territories, and its ability to enable repeated measures (immediately or as often as desired). Because ASL methods rely on a diffusible tracer, they are thus much less sensitive to vascular permeability than are large-molecule contrast material–dependent methods. The absence of contrast material with ASL also helps to remove uncertainties of risk, especially given new questions about the safety of some gadolinium-based preparations in individuals with renal impairment (31,32). Another important practical advantage of ASL is the immediate availability of perfusion images and the ease of quantification without extensive postprocessing.

There has been only limited clinical literature, to our knowledge, regarding ASL, and it is spread across multiple diseases (13,14,33–40). Indeed, the pri-

Figure 6

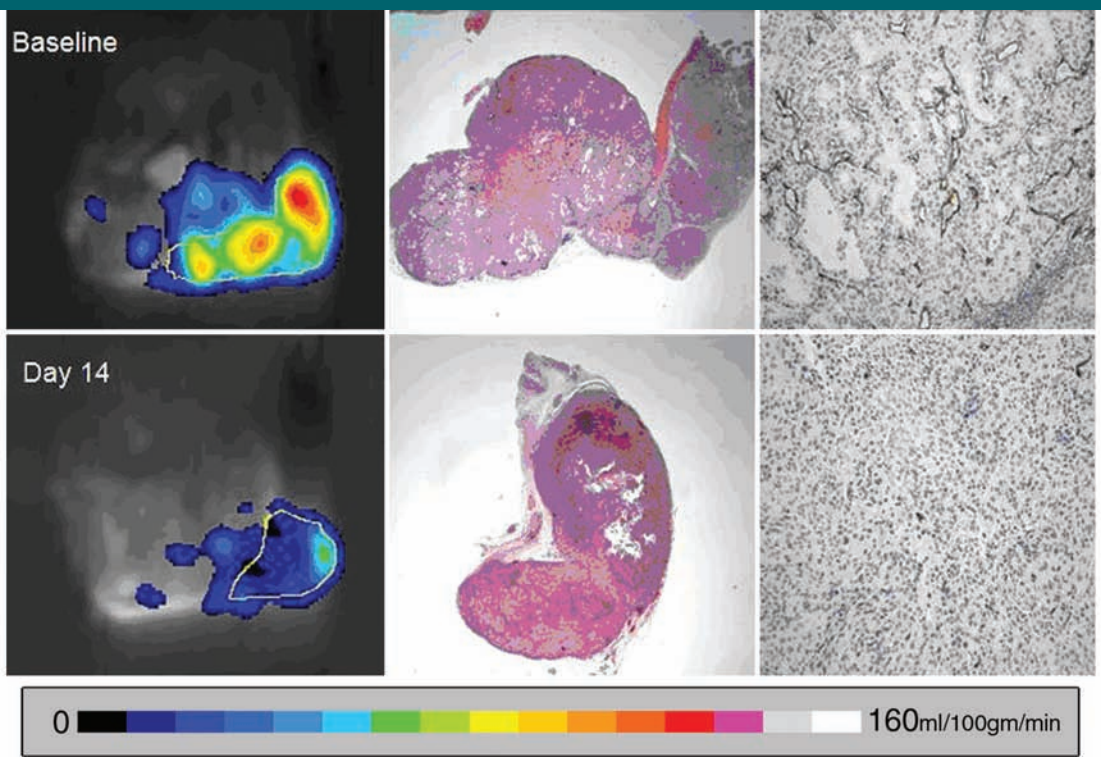

Figure 6: Histopathologic correlation of sorafenib-treated A498 tumors. Left: ASL perfusion maps (with yellow region of interest outlining the tumor). Middle: Hematoxylin-eosin–stained specimens. (Original magnification, ×2.) Right: Immunohistochemistry images. (CD34 stain; original magnification, ×20.) Color table represents flow values. *gm* = Gram.

mary application of ASL has been in the study of brain activation changes in healthy control subjects (13). Nevertheless, Silva et al (41) used an ASL technique to calculate blood flow within brain tumors in a rat glioma model. They showed that this method enables reliable repetitive quantifications of tumor blood flow, in addition to providing spatial information on the blood flow distribution. Warmuth et al (37) showed that ASL allows distinction between high- and low-grade gliomas and gives results comparable to those of dynamic susceptibility-weighted contrast material–enhanced MR imaging in the evaluation of tumor blood flow in patients with brain tumors. In their work, they highlighted that although blood flow is underestimated in low flow rates, only ASL yields absolute values that enable comparisons between patients (37). Similar results were reported by Wolf et al (38), who found strong correlation between the grade of the glioma and its maximal measured blood flow.

Another group (39) who studied meningiomas demonstrated significant correlation between the mean ASL signal intensity change in meningiomas and microvessel areas on histologic specimens (with CD31 staining). They also successfully used ASL to differentiate the angiomatous subtype of meningioma from the other subtypes.

Technical challenges concerning transit time artifact and the ability to label, or "tag," the supplying vessels of the tumor or organ have been overcome so that ASL can now be used for peripheral applications as well (42). Additionally, another prior limitation of ASL—its low signal-to-noise ratio—has been partially addressed by the use of increased magnetic field strengths (43). However, despite the potential of ASL for oncologic applications, both human and animal studies of ASL in this field are limited by small sample size, so that complete validation of the technique has not yet been achieved. Schmitt et al (40) evaluated the use of an ASL technique for the assessment of tissue perfusion in patients with head and neck carcinoma during radiation therapy. In their study, tumors with high initial perfusion tended to show better response to radiation therapy than those showing weak pretreatment perfusion. ASL has also been used to assess peripheral tumors such as RCC. De Bazelaire et al (14,44) have used it to monitor changes in RCC tumors receiving antiangiogenic (PTK787) therapy. Their findings further supported the correlation between early ASL characteristics at 1 month and later treatment response at 4 months.

In our study, each of the RCC xenografts we studied added information about how ASL could be used in the treatment of patients receiving antiangiogenic therapy. In the 786-0 tumors, absence of signal intensity correlated early with microvascular density and later with nonviability at hematoxylin-eosin staining. Return of peripheral signal intensity correlated with new growth and further showed that spatial (qualitative) information may be more important than global quantitative measurements. These results are in concordance with a recent study (45), where multisection CT perfusion was used to monitor antiangiogenic therapy in rodent R3230 adenocarcinomas. In that study, areas of increased perfusion developed even if the tumor had the same average blood flow, so that the spatial distribution of tumor blood flow appeared more important than quantitative values in detecting early changes in response to the antiangiogenic agent sorafenib. Thus, the combination of our and these prior results emphasize that identification of new signal intensity (ie, new zones of increased perfusion) over time is more important than absolute mean blood flow values in determining whether a specific tumor remains under control. In these models, such areas clearly represented the development of new vessels that occur despite the antiangiogenic therapy. These new vessels tended to develop at the periphery of the lesion in the 786-0 and R3230 models, whereas the A498 model had more central blood flow recurrence. This suggests that tumor-specific or host microenvironmental factors may be playing a role in the development of antiangiogenic resistance (46). Regardless, future clinical studies of the morphologic patterns of tumor growth with antian-

Figure 7

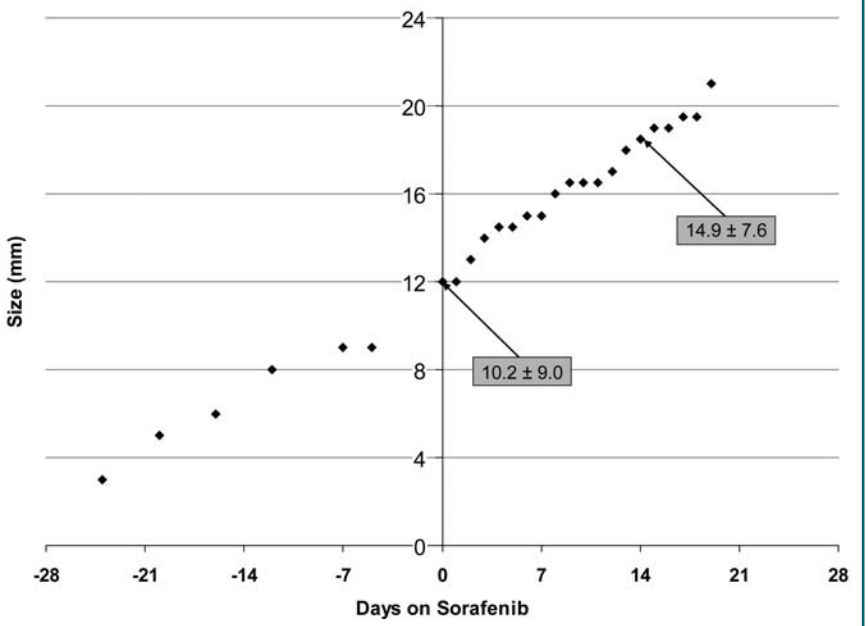

Figure 7: Average growth curve of Caki-1 cell line. Size was measured daily with calipers; mean blood flow values (in mL/100 g/min) presented in the shaded boxes were calculated from ASL MR images. No effect of sorafenib was seen for this cell line.

giogenic therapy and their clinical implications for different types of tumor are anticipated.

For at least one line (A498), ASL was an earlier predictor of developing resistance by 2–3 weeks, further suggesting that it may be a useful biomarker in some patients. Last, initial low-blood-flow signal intensity at ASL imaging in Caki-1 tumors was associated with no response to sorafenib, possibly suggesting that low ASL signal intensity at baseline (ie, <15 mL/100 g/min) may be used one day as a predictive biomarker for lack of responsiveness to antiangiogenic therapy. We attribute this finding to the fact that low ASL signal intensity likely represents more mature and/or fewer blood vessels in this tumor line that may potentially be less responsive to antiangiogenic therapy (14,22,47). Our study further sheds light as to why predictive and prognostic biomarkers will take on increasing importance. Indeed, our study results confirmed our prior unpublished observation of different responses to antiangiogenic therapy for three lines of RCC. The expansion of this technique and potential correlation of our results to additional RCC lines likely to be encountered in clinical practice clearly will be a priority for future study.

Although other perfusion parameters such as mean transit time exist (48), in our study we used blood flow values of tumor perfusion as measured at ASL MR imaging (in mL/100 g/min). Hence, controversy still exists as to which is the most accurate and clinically relevant of these parameters, and tumor perfusion varies greatly with the exact tumor type and even cell line. Accordingly, we are encouraged that the ASL values for tumor perfusion in our study and in a reported clinical trial (14,44) compare well with results from a positron emission tomographic (PET) study of blood flow in human renal cell primary cancers and metastases (49). Yet our values are slightly lower than the values obtained in a CT study of human renal cell metastases (50), potentially because of any of the well-known differences between animal models and clinical practice (eg, cell type, location). In regard to animal studies and alternative methods for measuring blood flow and perfusion, Hines-Peralta et al (51) previously used laser Doppler in renal cell xenografts, but this method did not provide reliable absolute measurement. Measures of blood volume and permeability have been reported in a murine renal cell cancer model (52), but measurement of blood flow was limited to measurement of relative changes in the supplying arterial velocity by using ultrasonography. On the other hand, as noted above, the greatest radiologic-pathologic correlation, particularly for spatial accuracy, was noted between CT perfusion and blood flow in a rat mammary adenocar-

Figure 8

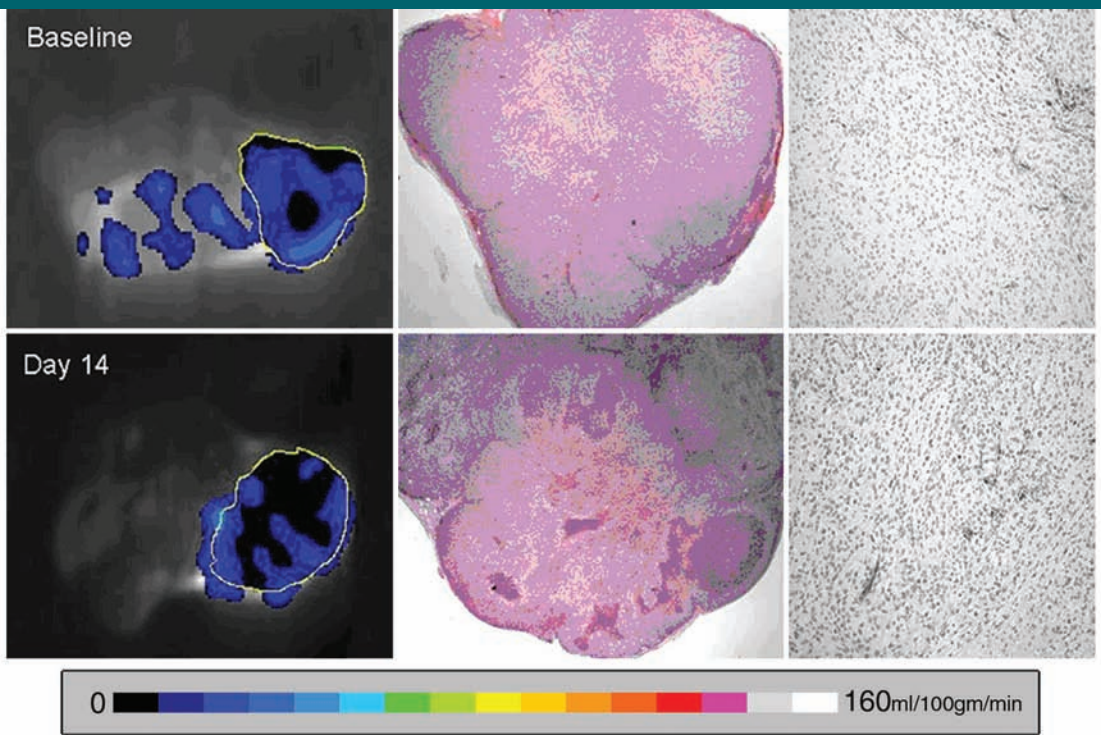

Figure 8: Histopathologic correlation of sorafenib-treated Caki-1 tumors. Left: ASL perfusion maps (with yellow region of interest outlining the tumor). Middle: Hematoxylin-eosin–stained specimen (entire specimen is tumor). (Original magnification, ×2.) Right: Immunohistochemistry images. (CD34 stain; original magnification, ×20.) Color table represents flow values. *gm* = Gram.

cinoma model (45), further supporting the relevancy of our approach.

There were several limitations of our study. Our study was performed by using only one animal model, with a limited number of cell lines that may not be representative of the spectrum of tumors encountered in clinical practice. Additionally, a small sample size per each cell line was employed. We also used a single antiangiogenic agent, sorafenib, and it must be acknowledged that other antiangiogenic agents, such as sunitinib (6), may produce different effects.

Furthermore, in our study, we used a single 2-mm section at the greatest tumor diameter. The use of a single section and its thickness was driven by the model size we used (tumors of 12–20 mm) and by the specific coil that was built to accommodate it. Yet the use of a single section adds a potential complexity when studying a subject at more prolonged follow-up intervals; as the tumors may change in shape, size, or orientation, the patient may not be oriented in the exact same position, thereby rendering the single section nonrepresentative. Because a key finding of our work was that characteristics of the tumor during treatment are spatially heterogeneous, it is clear that imaging only a single section through the tumor was a limitation of our study. Enhancements to the ASL measurement method to enable multisection measurement, as have been developed for human brain studies (53), are clearly desirable.

Additional studies need to be performed as further research is warranted. To assess the effect of host microenvironment and to precisely determine the relevance of our findings to clinical practice, we plan to next study different strains of tumors and animals and the effect of tumor location. Next, other clinically approved antiangiogenic drugs such as sunitinib (6) will be studied. We further plan to check the utility of ASL in looking at combined treatments, such as radiation therapy and antiangiogenic drugs. Future work emphasizing localized correlation between quantitative histopathologic measures and imaging markers, such as that reported by Hoskin et al (54) in prostate cancer, would permit better determination of the relationship between flow and proliferating tumor physiology. Last, further studies of ASL imaging should ultimately include comparison to other physiologic imaging methods, such as dynamic contrast-enhanced MR imaging (37,37), CT perfusion (10,11,24,48), and PET, to compare accuracy, clinical benefits, and disadvantages of each method in controlled animal studies and ultimately in clinical practice.

In conclusion, our study showed radiologic-pathologic validation of ASL MR imaging for the monitoring of antiangiogenic therapy in murine xenograft tumor models and highlighted potential roles for ASL in clinical practice. Specifically, this tight correlation suggests the potential for ASL MR imaging results to function as a surrogate marker for the treatment of patients with cancer receiving antiangiogenic agents such as sorafenib. Indeed, our results add to the growing body of literature that shows why currently available systems for tumor monitoring (such as the Response Evaluation Criteria in Solid Tumors guidelines) may not be reliable as the sole criteria for assessing therapeutic efficacy when using agents that reduce tumor blood flow, because changes in blood flow did not always match changes in tumor growth. Furthermore, as our results in A498 tumors showed, growth in tumor size may not signify the earliest assessable development of resistance. It is therefore important to emphasize the need to perform both anatomic and physiologic measurements in following such patients. For low-blood-flow tumors, such as Caki-1, ASL MR imaging can possibly help predict the lack of responsiveness to antiangiogenic therapy. Thus, if characterized and validated, ASL MR imaging may one day be used as an important guide on which to base therapeutic decisions for patients with RCC and others receiving antiangiogenic therapy.

References

1. Wilhelm SM, Carter C, Tang L, et al. BAY 43–9006 exhibits broad spectrum oral antitumor activity and targets the RAF/MEK/ERK pathway and receptor tyrosine kinases involved in tumor progression and angiogenesis. Cancer Res 2004;64(19):7099–7109.

2. Kane RC, Farrell AT, Saber H, et al. Sorafenib for the treatment of advanced renal cell carcinoma. Clin Cancer Res 2006;12(24):7271–7278.

3. Schoffski P, Dumez H, Clement P, et al. Emerging role of tyrosine kinase inhibitors in the treatment of advanced renal cell cancer: a review. Ann Oncol 2006;17(8):1185–1196.

4. Garcia JA, Rini BI. Recent progress in the management of advanced renal cell carcinoma. CA Cancer J Clin 2007;57(2):112–125.

5. Oudard S, George D, Medioni J, Motzer R. Treatment options in renal cell carcinoma: past, present and future. Ann Oncol 2007; 18(suppl 10):x25–x31.

6. Costa LJ, Drabkin HA. Renal cell carcinoma: new developments in molecular biology and potential for targeted therapies. Oncologist 2007; 12(12):1404–1415.

7. Escudier B, Eisen T, Stadler WM, et al; for the TARGET Study Group. Sorafenib in advanced clear-cell renal-cell carcinoma. N Engl J Med 2007;356(2):125–134.

8. Sosman JA, Puzanov I, Atkins MB. Opportunities and obstacles to combination targeted therapy in renal cell cancer. Clin Cancer Res 2007; 13(2 pt 2):764s–769s.

9. Therasse P, Eisenhauer EA, Verweij J. RECIST revisited: a review of validation studies on tumor assessment. Eur J Cancer 2006;42(8): 1031–1039.

10. Sahani DV, Kalva SP, Hamberg LM, et al. Assessing tumor perfusion and treatment response in rectal cancer with multisection CT: initial observations. Radiology 2005;234(3): 785–792.

11. Cuenod CA, Fournier L, Balvay D, Guinebretiere JM. Tumor angiogenesis: pathophysiology and implication for contrast-enhanced MRI and CT assessment. Abdom Imaging 2006;31(2):188–193.

12. Kan Z, Phongkitkarun S, Kobayashi S, et al. Functional CT for quantifying tumor perfusion in antiangiogenic therapy in a rat model. Radiology 2005;237(1):151–158.

13. Detre JA, Alsop DC. Perfusion magnetic resonance imaging with continuous arterial spin labeling: methods and clinical application in the central nervous system. Eur J Radiol 1999; 30(2):115–124.

14. De Bazelaire C, Rofsky NM, Duhamel G, Michaelson MD, George D, Alsop DC. Arterial spin labeling blood flow magnetic resonance imaging for the characterization of metastatic renal cell carcinoma. Acad Radiol 2005;12(3): 347–357.

15. Haviv YS, van Houdt WJ, Lu B, Curiel DT, Zhu ZB. Transcriptional targeting in renal cancer cell lines via the human CXCR4 promoter. Mol Cancer Ther 2004;3(6):687–691.

16. Ye FQ, Frank JA, Weinberger DR, McLaughlin AC. Noise reduction in 3D perfusion imaging by attenuating the static signal in arterial spin tagging (ASSIST). Magn Reson Med 2000;44(1):92–100.

17. Kwong KK, Chesler DA, Weisskoff RM, et al. MR perfusion studies with T1-weighted echo planar imaging. Magn Reson Med 1995;34(6):878–887.

18. Ordidge RJ, Wylezinska M, Hugg JW, Butterworth E, Franconi F. Frequency offset corrected inversion (FOCI) pulses for use in localized spectroscopy. Magn Reson Med 1996;36(4):562–566.

19. Yongbi MN, Yang Y, Frank JA, Duyn JH. Multislice perfusion imaging in human brain using the C-FOCI inversion pulse: comparison with hyperbolic secant. Magn Reson Med 1999;42(6):1098–1105.

20. Garcia DM, Duhamel G, Alsop DC. Efficiency of inversion pulses for background suppressed arterial spin labeling. Magn Reson Med 2005;54(2):366–372.

21. Wong EC, Buxton RB, Frank LR. Quantitative imaging of perfusion using a single substraction (QUIPSS and QUIPSS II). Magn Reson Med 1998;39(5):702–708.

22. Alsop DC, Detre JA. Reduced transit-time sensitivity in noninvasive magnetic resonance imaging of human cerebral blood flow. J Cereb Blood Flow Metab 1996;16(6):1236–1249.

23. Willett CG, Boucher Y, di Tomaso E, et al. Direct evidence that the VEGF-specific antibody bevacizumab has antivascular effects in human rectal cancer. Nat Med 2004;10(2):145–147.

24. Li ZP, Meng QF, Sun CH, et al. Tumor angiogenesis and dynamic CT in colorectal carcinoma: radiologic-pathologic correlation. World J Gastroenterol 2005;11(9):1287–1291.

25. Brix G, Bahner ML, Hoffmann U, Horvath A, Schreiber W. Regional blood flow, capillary permeability, and comprtmental volumes: measurement with dynamic CT—initial experience. Radiology 1999;210(1):269–276.

26. Wong GT, Irwin MG. Contrast-induced nephropathy. Br J Anaesth 2007;99(4):474–483.

27. Toprak O. Risk markers for contrast-induced nephropathy. Am J Med Sci 2007;334(4):283–290.

28. Katzberg RW, Barrett BJ. Risk of iodinated contrast material–induced nephropathy with intravenous administration. Radiology 2007;243(3):622–628.

29. Walsh EG, Minematsu K, Leppo J, Moore SC. Radioactive microsphere validation of a volume localized continuous saturation perfusion measurement. Magn Reson Med 1994;31(2):147–153.

30. Ewing JR, Wei L, Knight RA, et al. Direct comparison of local cerebral blood flow rates measured by MRI arterial spin-tagging and quantitative autoradiography in a rat model of experimental cerebral ischemia. J Cereb Blood Flow Metab 2003;23(2):198–209.

31. Thomsen HS. Gadolinium-based contrast media may be nephrotoxic even at approved doses. Eur Radiol 2004;14(9):1654–1656.

32. Erley CM, Bader BD, Berger ED, et al. Gadolinium-based contrast media compared with iodinated media for digital subtraction angiography in azotaemic patients. Nephrol Dial Transplant 2004;19(10):2526–2531.

33. Jahng GH, Zhu XP, Matson GB, Weiner MW, Schuff N. Improved perfusion-weighted MRI by a novel double inversion with proximal labeling of both tagged and control acquisitions. Magn Reson Med 2003;49(2):307–314.

34. Kim HS, Kim SY. A prospective study on the added value of pulsed arterial spin-labeling and apparent diffusion coefficients in the grading of gliomas. AJNR Am J Neuroradiol 2007;28(9):1693–1699.

35. Chalela JA, Alsop DC, Gonzalez-Atavales JB, Maldjian JA, Kasner SE, Detre JA. Magnetic resonance perfusion imaging in acute ischemic stroke using continuous arterial spin labeling. Stroke 2000;31(3):680–687.

36. Detre JA, Alsop DC, Vives LR, Maccotta L, Teener JW, Raps EC. Noninvasive MRI evaluation of cerebral blood flow in cerebrovascular disease. Neurology 1998;50(3):633–641.

37. Warmuth C, Gunther M, Zimmer C. Quantification of blood flow in brain tumors: comparison of arterial spin labeling and dynamic susceptibility-weighted contrast-enhanced MR imaging. Radiology 2003;228(2):523–532.

38. Wolf RL, Wang J, Wang S, et al. Grading of CNS neoplasms using continuous arterial spin labeled perfusion MR imaging at 3 Tesla. J Magn Reson Imaging 2005;22(4):475–482.

39. Kimura H, Takeuchi H, Koshimoto Y, et al. Perfusion imaging of meningioma by using continuous arterial spin-labeling: comparison with dynamic susceptibility-weighted contrast-enhanced MR images and histopathologic features. AJNR Am J Neuroradiol 2006;27(1):85–93.

40. Schmitt P, Kotas M, Tobermann A, Haase A, Flentje M. Quantitative tissue perfusion measurments in head and neck carcinoma patients before and during radiation therapy with a non-invasive MR imaging spin-labeling technique. Radiother Oncol 2003;67(1):27–34.

41. Silva AC, Kim SG, Garwood M. Imaging blood flow in brain tumors using arterial spin labeling. Magn Reson Med 2000;44(2):169–173.

42. Barrett T, Brechbiel M, Bernardo M, Choyke PL. MRI of tumor angiogenesis. J Magn Reson Imaging 2007;26(2):235–249.

43. Petersen ET, Zimine I, Ho YC, Golay X. Non-invasive measurement of perfusion: a critical review of arterial spin labelling techniques. Br J Radiol 2006;79(944):688–701.

44. De Bazelaire C, Alsop DC, George D, et al. Magnetic resonance imaging-measured blood flow change after antiangiogenic therapy with PTK787/ZK 222584 correlates with clinical outcome in metastatic renal cell carcinoma. Clin Cancer Res 2008;14(17):5548–5554.

45. Sabir A, Schor-Bardach R, Wilcox CJ, et al. Multislice CT perfusion imaging enables early detection of therapeutic response to antiangiogenic therapy. AJR Am J Roentgenol 2008;191(1):133–139.

46. Nyberg P, Salo T, Kalluri R. Tumor microenviroment and angiogenesis. Front Biosci 2008;13:6537–6553.

47. Matsumoto S, Hyodo F, Subramanian S, et al. Low-field paramagnetic resonance imaging of tumor oxygenation and glycolytic activity in mice. J Clin Invest 2008;118(5):1965–1973.

48. Zhu AX, Holalkere NS, Muzikansky A, Horgan K, Sahani DV. Early antiangiogenic activity of bevacizumab evaluated by computed tomography perfusion scan in patients with advanced hepatocellular carcinoma. Oncologist 2008;13(2):120–125.

49. Anderson H, Yap JT, Wells P, et al. Measurement of renal tumour and normal tissue perfusion using positron emission tomography in a phase II clinical trial of razoxane. Br J Cancer 2003;89(2):262–267.

50. Faria SC, Ng CS, Hess KR, et al. CT quantification of effects of thalidomide in patients with metastatic renal cell carcinoma. AJR Am J Roentgenol 2007;189(2):378–385.

51. Hines-Peralta A, Sukhatme V, Regan M, Signoretti S, Liu ZJ, Goldberg SN. Improved tumor destruction with arsenic trioxide and radiofrequency ablation in three animal models. Radiology 2006;240(1):82–89.

52. Drevs J, Hofmann I, Hugenschmidt H, et al. Effects of PTK787/ZK 222584, a specific inhibitor of vascular endothelial growth factor receptor tyrosine kinases, on primary tumor, metastasis, vessel density, and blood flow in a murine renal cell carcinoma model. Cancer Res 2000;60(17):4819–4824.

53. Alsop DC, Detre JA. Multisection cerebral blood flow MR imaging with continuous arterial spin labeling. Radiology 1998;208(2):410–416.

54. Hoskin PJ, Carnell DM, Taylor NJ, et al. Hypoxia in prostate cancer: correlation of BOLD-MRI with pimonidazole immunohistochemistry—initial observations. Int J Radiat Oncol Biol Phys 2007;68(4):1065–1071.